10.1098/rsta.2000.0809

THE ROYAL SOCIETY

Entropically driven self-assembly and interaction in suspension

BY A. G. YODH, KENG-HUI LIN, JOHN C. CROCKER†, A. D. DINSMORE‡, RITU VERMA¶ AND P. D. KAPLAN¶

Department of Physics and Astronomy, University of Pennsylvania, Philadelphia, PA 19104-6396, USA

In this paper we present fundamental studies elucidating the role of entropy in particle suspensions. We focus on systems composed of large colloidal particles along with a second, usually smaller species such as a particle or polymer. We describe direct measurements of these interactions in suspension, and we systematically show how these forces can be used to control the self-assembly of colloidal particles. The paper provides a unified review of the experiments from our laboratory, and in a few cases touches on very recent results.

Keywords: entropy; colloids; suspensions; self-assembly; polymers; templating

1. Introduction

Entropic forces between macromolecules in suspension are sometimes produced by the addition of other constituents to the background solvent. These added constituents are often other (usually smaller) particles, rods or polymers. The resulting entropic forces influence suspension stability, and are of considerable importance in a wide variety of practical materials ranging from frozen desserts to paints to motor oils to living cells. During the last few years we have been studying entropic effects in suspension. We have quantified these forces by direct measurement in a variety of complex fluids, we have identified some novel manifestations of these entropic phenomena, and we have used these effects to control the self-assembly of particles. In this paper we provide a unified review of the experiments from our laboratory, and in a few cases touch on very recent results.

The starting point of our exposition naturally begins with mixtures of large- and small-diameter hard spheres. Hard-sphere colloids lack attractive and long-range interactions, which typically compete with entropic effects to produce ordered phases. Nonetheless, as Asakura & Oosawa (1958) first noted, in mixtures of *different-sized* spherical particles, an *ordered* arrangement of large spheres can *increase* the total entropy of the system by increasing the entropy of the small spheres. This phenomenon is depicted in figure 1. Because the centre of mass of the small sphere

† Present address: Applied Physics Department, California Institute of Technology, Pasadena, CA 91125, USA.

‡ Present address: Division of Engineering and Applied Science, Harvard University, Cambridge, MA 02138, USA.

¶ Present address: Unilever Research US, 45 River Rd, Edgewater, NJ 07020, USA.

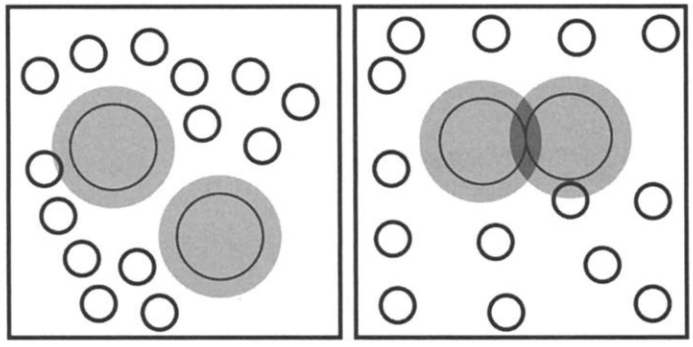

Figure 1. Schematic of large and small spheres in suspension showing the excluded volume regions described in the text. The light shaded region is the space excluded to the small-sphere centres, and the heavy shaded region represents the increase in volume available to the small spheres when these excluded volumes overlap.

cannot penetrate within $\frac{1}{2}a_S$ of the large-sphere surface, a region of 'excluded volume' surrounds each large sphere (here, a_S and a_L are the diameters of the small and large spheres, respectively). When the surfaces of the two large spheres approach within a small-sphere diameter, these excluded volume regions overlap one another, and the total volume accessible to the centre of mass of the small spheres increases. The resulting increase in small-sphere entropy induces the so-called attractive 'depletion' force between the large spheres. At low concentrations of small spheres, simple models (Asakura & Oosawa 1958; Vrij 1976; Gast *et al.* 1983) predict that this energy of attraction is proportional to the volume fraction of the small spheres (Φ_S), and to the ratio of large- (a_L) to small-sphere (a_S) diameter. The attraction energy at contact is *ca.* $\frac{3}{2}(a_L/a_S)\Phi_S k_B T$, where k_B is the Boltzmann constant and T the ambient temperature. This attraction energy can be several $k_B T$ in practice. It has been observed to drive phase separation in monodisperse colloids with added polymer (Ilett *et al.* 1995; Poon & Warren 1994; Poon *et al.* 1994, 1997; Calderon *et al.* 1993; De Hek & Vrij 1981), in monodisperse emulsions with added polymer (Bibette *et al.* 1990, 1992), in binary emulsions (Steiner *et al.* 1995), and in suspensions of silica and polystyrene spheres (Kaplan *et al.* 1994; Dinsmore *et al.* 1995; Sanyal *et al.* 1992; van Duijneveldt *et al.* 1993).

2. Direct measurements of entropic potentials of mean force

We have developed a simple experimental apparatus to directly measure particle interaction potentials in suspension. Using the instrument we have studied entropic interaction potentials brought about by added particles (Crocker *et al.* 1999), polymers (Verma *et al.* 1998, 2000) and rods. We have studied dilute samples for which 'ideal-gas-type' models might be expected to provide a good approximation of the physical system, and we have studied more concentrated samples wherein correlation effects characteristic of the background fluids influence the particle interactions. Our observations reveal information about colloid interactions, and about the physics of the background medium. In our most accurate measurements, the energy resolution was *ca.* $0.05 k_B T$ and the spatial resolution, i.e. the accuracy of our determination of centre-to-centre particle separation, was *ca.* 15 nm.

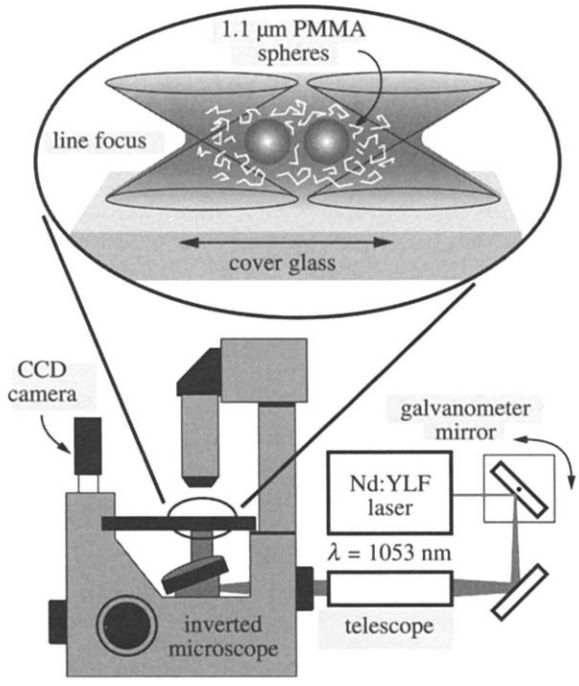

Figure 2. Experimental set-up. The inset shows two spheres in the scanning trap.

Data were collected by video microscopy using the microscope and optical tweezer system represented schematically in figure 2. Optical tweezers exploit optical gradient forces to trap dielectric particles in three dimensions near the waist of a strongly focused laser beam (Ashkin *et al.* 1986; Afzal & Treacy 1992). We scan the focus from side to side, rapidly enough that the particle cannot follow the trap and so responds to the time-averaged optical field. The effective trapping potential is thus confined to a line within the sample, and hence we call it a line optical tweezer. In this trap, micron-sized colloidal spheres are free to diffuse in one dimension, along the scan direction, while being strongly confined in the two perpendicular directions. The particles act as if they are threaded on a frictionless rod of light. The effective interaction potential of the two spheres, $U(r)$, is related to the probability, $P(r)$, of finding the two spheres with centres separated by a distance r. We use the Boltzmann relation to extract this potential of mean force from the measured probability distribution, i.e. $P(r) \propto \exp\{-U(r)/k_{\mathrm{B}}T\}$. We estimate $P(r)$ from a histogram of the measured pair separations. Thirty minutes of videotape yields *ca.* 10^5 image fields (i.e. separation measurements) for histogramming.

Two properties of the line tweezer are essential to our potential measurement. First, the tweezer-induced forces, along the line adjoining the sphere centres, are weak enough to be easily subtracted from the measured free energy. Second, the tweezer strongly confines both spheres to the microscope focal plane, allowing us to equate the in-plane separation measured from a video image to the spheres' actual three-dimensional separation. A less critical feature of the line tweezer is that by adjustment of the scan rate waveform one can create a harmonic optical potential well near the centre of the line; this keeps the particles closer together and speeds up

the data-collection process. The instrument was also susceptible to a few systematic errors. At close range, accurate measurement of separation was complicated by the overlap of particle diffraction patterns. We devised a simple image-correction procedure to improve our estimate of the true particle centroids (Crocker *et al.* 1999; Verma *et al.* 2000); ultimately this approximate procedure limited the spatial resolution of these experiments. In addition, the scanned optical tweezer can 'kick' the beads (Faucheux *et al.* 1995*a*, *b*) in the scan direction. For our fast bidirectional scanning the small kicks tend to cancel each other out, leaving unbiased Brownian motion. Typically, in order to elucidate the effects of suspension additives, we performed control measurements on isolated particles in a suspension and subtracted the resulting 'background potentials' from our experimental data. This subtraction further reduced the effects of trap-induced systematic errors.

The samples were housed in cells consisting of a microscope slide and cover glass with a 120 μm thick Parafilm spacer. The trapped particles were *ca.* 1.1 μm diameter silica or polymethylmethacrylate (PMMA) spheres. These spheres behaved approximately as hard spheres. The line trap was derived from *ca.* 50 mW of the CW output of a Nd:YLF laser (1054 nm wavelength), and was scanned back and forth at *ca.* 180 Hz. The line was *ca.* 10 μm long. The trap was typically located *ca.* 3 μm below the cover glass surface. This distance was chosen to minimize possible hydrodynamic and electrostatic wall effects, and at the same time minimize out-of-plane particle motion due to the weakening of the trap by spherical aberration. We carefully regulated sphere–wall separation and laser power during the course of the experiment to keep trapping characteristics constant.

The first set of results we derived with the instrument (see figure 3) directly corroborated the theory of Asakara and Oosawa (AO theory; see Asakura & Oosawa (1958); see also Vrij (1976)) in suspensions of large and small hard spheres at low volume fractions, and revealed some interesting new effects at higher concentrations of the small spheres (Crocker *et al.* 1999). In figure 3*a* the measured large-sphere potential of mean force is presented for values of small-sphere volume fraction (Φ_S) ranging from 0 to 0.42. The most prominent feature in these potentials is the attraction at short range. AO theory predicts an attraction of the form:

$$U(r) = \Pi(\tfrac{1}{6}\pi a_S^3)\left[\frac{\lambda}{\lambda-1}\right]^3\left[1-\left(\frac{3r}{2a_L\lambda}\right)+\frac{1}{2}\left(\frac{r}{a_L\lambda}\right)^3\right]. \tag{2.1}$$

Here Π is the osmotic pressure of the small particles, $\lambda = 1+(a_S/a_L)$, and the large-particle centre-to-centre separation, r, lies between a_L and $(a_L + a_S)$. We attempted to fit data at the lowest small-sphere volume fractions ($\Phi_S = 0.04, 0.07$) with the theory of Asakura & Oosawa (1958). The best fits to the AO model are shown as solid lines in figure 3*b*. To obtain these nearly perfect fits we had to adjust the small-sphere radius slightly, from *ca.* 42 nm (number provided by the manufacturer) to *ca.* 49 nm. This increase in effective small-sphere size was readily accounted for by the screened electrostatic repulsion (*ca.* 3 nm in our samples) as well as a very small additional swelling of the particle.

At higher small-particle concentrations their liquid structure becomes important (Dickman *et al.* 1997; Gotzelmann *et al.* 1998; Chu *et al.* 1996; Biben *et al.* 1996; Piasecki *et al.* 1995; Mao *et al.* 1997). We see that when $\Phi_S > 0.1$, there is a substantial depletion repulsion at separations of the order of one small-sphere diameter from contact. The AO model does not predict this repulsion. Qualitatively, the effect

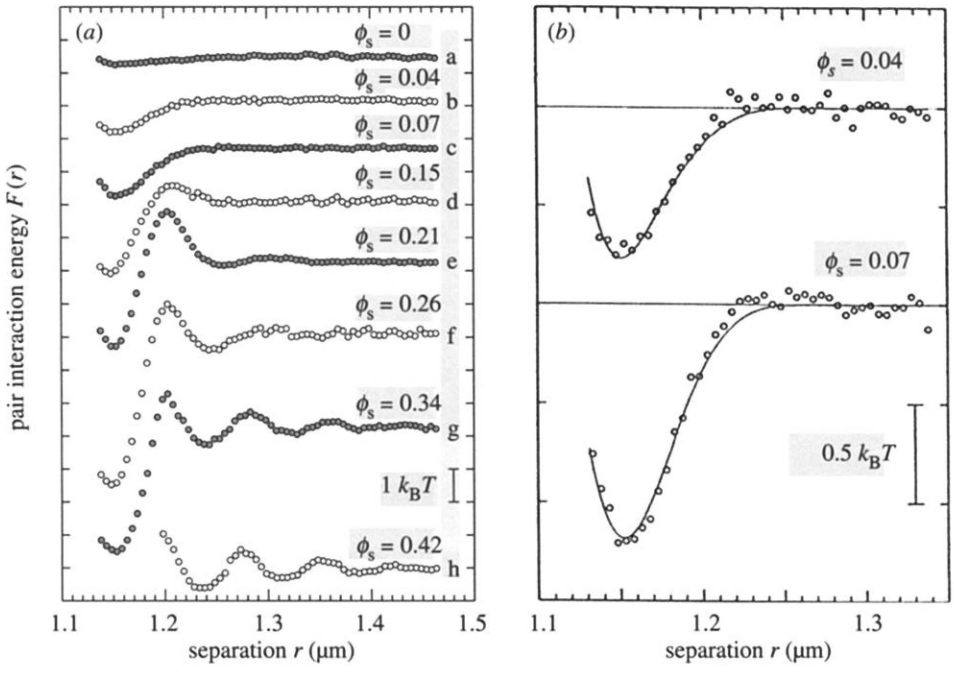

Figure 3. (*a*) The entropic interaction potentials measured with small-sphere volume fractions ranging from $\Phi_S = 0$ to 0.42 (the large-sphere volume fraction was less than 10^{-7}). At the lowest volume fractions (curves b and c), the potential is monotonically attractive, resembling the Asakura–Oosawa depletion model. As more spheres are added, a repulsive barrier forms (curves d and e), then a secondary minimum (curve f), and finally the potential becomes becoming fully oscillatory (curves g and h). The spheres associated with curve h never reached the primary depletion minimum. (*b*) Data for $\Phi_S = 0.04$ and $\Phi_S = 0.07$ with the background potential ($\Phi_S = 0$) subtracted. The upturn on the leftmost end of the curves is due to the resolution-broadened bare repulsion of the two spheres. The curves are fits to the Asakura–Oosawa model, blurred with a Gaussian kernel to account for our instrumental resolution.

arises because the small spheres tend to form in layers around the large spheres. When the gap between the large spheres is commensurate with these layers, the free energy is lower; when the gap is incommensurate, the energy is higher. For $\Phi_S \geqslant 0.25$, the effect of the higher-order small-particle shells becomes significant, making the potential oscillatory with wavelength comparable with the mean spacing in the small-sphere fluid. At these higher small-particle volume fractions, the two large spheres were very rarely thermally activated into the primary depletion minimum. At the highest Φ_S, the large particles were never activated (during experiments of *ca.* 3 h in duration) into the primary minimum. It is possible that this anomalous slowing of thermal activation is kinetic or hydrodynamic in origin; the phenomena might be better understood in simulations that include particle dynamics. Taken together these results suggest that concentrated systems of hard spheres are replete with slowly evolving, metastable particle configurations.

In a second set of measurements, we explored the attraction between large spheres in polymer solutions (Verma *et al.* 1998, 2000). When the polymer solution is dilute, the polymers are readily modelled as an ideal gas of hard spheres with mean size

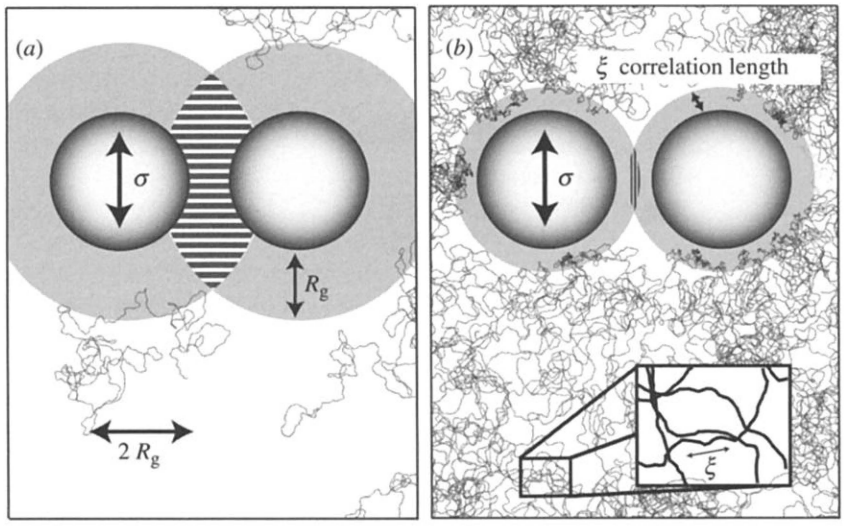

Figure 4. Polymer depletion in the (*a*) dilute and (*b*) semi-dilute regimes. The depletion region is shaded grey, and the hatched region corresponds to the increase in volume accessible to the polymers when the particles move sufficiently close to one another.

proportional to the radius of gyration (R_g) of the polymers. Unlike the hard spheres, polymers in solution can interpenetrate, significantly reducing any effects due to liquid structure that we discussed above. In this regime the AO model should work. As the polymer concentration is increased, however, the coils begin to overlap and entanglement effects become important. We were particularly interested in understanding how the attraction between particles is modified by polymer entanglement effects that arise when the polymer concentration is increased above the critical overlap concentration C^*. Such *semi-dilute* polymer solutions are characterized by a correlation length ξ rather than by R_g. The length-scale ξ can be thought of as the average spatial distance between neighbouring entanglement points. If the polymer–colloid interaction is repulsive (i.e. if the polymer does not adsorb to the particles), then a polymer-depleted 'correlation cavity' with thickness proportional to ξ (Joanny *et al.* 1979; Grosberg & Khokhlov 1994) develops around the particle, and depletion attraction should still occur (see figure 4).

Our experiments employed silica spheres in polymeric solutions of λ-DNA. λ-DNA is a non-adsorbing semi-flexible polymer with persistence length *ca.* 50 nm and a contour length of 16.5 μm. The measured interaction potentials as a function of DNA concentration are shown in figure 5. At the lower concentrations the AO model can be used to fit the data, and it provides reasonable agreement given the experimental resolution. Above C^* the potentials of mean force become deeper and shorter in range. How can we understand these semi-dilute data more quantitatively? In semi-dilute solutions the intersphere potential has been predicted (Joanny *et al.* 1979) within the Derjaguin approximation. Within this approximation, the form of the potential of mean force between particles in the semi-dilute polymer is the same as that of the AO model (equation (2.1)) to lowest order in $[r-(a_L+a_S)]$, provided a_S is replaced by $(\pi\xi)$, and provided that the ideal gas osmotic pressure in equation (2.1) (proportional to small-sphere number density) is changed to that of the polymer

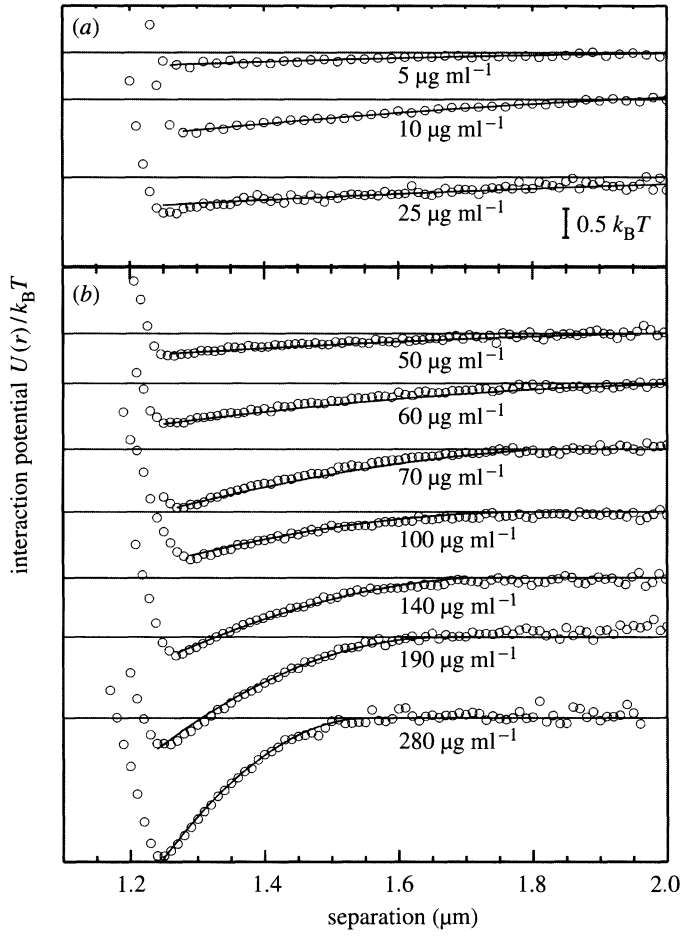

Figure 5. Interaction potential between two 1.25 μm silica spheres in (*a*) the dilute and (*b*) the semi-dilute region. The dimensionless potential, $U(r)/k_BT$, is plotted as a function of r, the interparticle distance. The open circles are data points, and the solid lines are fits to the AO model, as described in the text.

solution (proportional to the polymer concentration raised to a power that depends on the phase of the polymer solution). The solid lines in figure 5 are best fits to the data using this semi-dilute model (Joanny *et al.* 1979), which is effectively a rescaled AO model. There are two free parameters in these fits, ξ and Π; both parameters depend on DNA concentration.

In figure 6 we plot ξ and Π as a function of polymer (DNA) coil density. Within our error limits, the data at low concentration agree with what we expect for an ideal gas of polymer coils. Notice, however, that the dependence of these quantities on coil density changes markedly near C^*. For example, the correlation length scales with the reciprocal of the square root of the coil density in the semi-dilute regime. This density dependence provides strong evidence of a transition from a dilute solution of Gaussian coils to a semi-dilute regime dominated by pair-wise contacts (Schaefer *et al.* 1980; Grosberg & Khokhlov 1994). This transition has been predicted to exist *only for semiflexible polymers* (Schaefer *et al.* 1980; Grosberg & Khokhlov 1994). Since

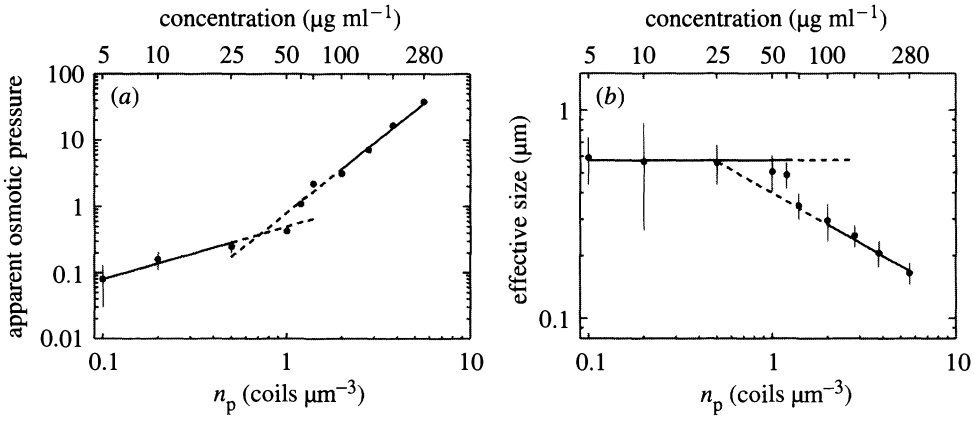

Figure 6. (*a*) Scaling behaviour of the osmotic pressure as a function of polymer concentration. The vertical axis represents Π/k_BT, and the horizontal axis is concentration in units of number density. (*b*) The filled circles represent the range of the potential, i.e. the fit parameter '$\frac{1}{2}a_S$' in the dilute regime or ξ in the semi-dilute regime. The crossover concentration C^* from dilute to semi-dilute regimes occurs at *ca.* 1.0 μm^{-3} on the horizontal axis.

the microscopic parameters (e.g. diameter, persistence length, etc.) of λ-DNA have been determined by many qualitatively different measurements (Taylor & Hagerman 1990; Schmidt 1973; Dauson & Harpst 1971; Arutyunyan *et al.* 1993; Pernodet & Tinland 1997; Baumann *et al.* 1997), we were able to map out the phase diagram of our polymer solutions, and together with our observations, confirm the existence of this transition, which depends on polymer flexibility (Verma *et al.* 2000).

Lastly, we have undertaken measurements of the depletion potential resulting from a background suspension of rods. For these experiments we use silica spheres and fd-virus (rods). The rods are monodisperse, *ca.* 880 nm in length, and have been used extensively in self-assembly experiments (Fraden *et al.* 1993; Stroobants *et al.* 1986; Smith 1970; Adams *et al.* 1998; Vliegenthart & Lekkerkerker 1999; van Bruggen *et al.* 1996; Dogic & Fraden 1997; Tang & Fraden 1995). Figure 7 exhibits a preliminary measurement of the effect at relatively low rod volume fraction. Also shown on the plot are two curves. One curve (solid) is the recent theoretical prediction of the sphere attraction due to rod depletion (Yaman *et al.* 1998), valid outside of the Derjaguin limit. The other curve (dash–dot) is the AO model prediction using the same *volume fraction* of background constituents, and assuming a background sphere diameter of 880 nm. The shape of the data fits the rod depletion much better than the sphere model. Furthermore, the entropic effect of the rods is much more substantive than the spheres given the same *volume* of material (see also Mao *et al.* 1995; Bolhuis *et al.* 1997).

To conclude this section, we note that the combination of the line optical tweezer and video microscopy provides a relatively straightforward means of directly determining the depth and shape of the potentials of mean force between particles in suspension. These model-independent potentials ultimately enable us to quantify the microscopic interactions in suspension that affect a broad range of self-assembly phenomena. The results described above have focused on entropic interactions, but the scheme is readily accessible to other types of problem. Interestingly, we have also

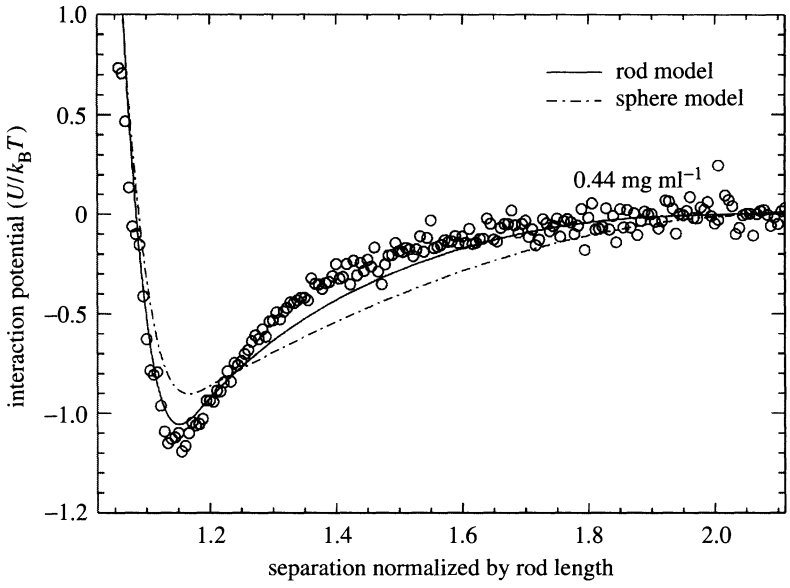

Figure 7. The interaction potential between 1.0 μm diameter silica spheres in a suspension of rods. The rods are fd-virus with length $L = 880$ nm, and diameter $d \sim 6.6$ nm. The weight fraction of the fd-virus is 0.44 mg ml^{-1}, corresponding to a number density of *ca.* 18 fd-virus per cubic micron. The dimensionless potential $U(r)/k_BT$ is plotted as a function of r/L, the particle centre-to-centre separation normalized by the rod length. The open circles are data points. The solid line is a theoretical prediction for rods under these conditions (Yaman *et al.* 1998). The dot-dashed line is *ca.* 1000 times the prediction of an AO hard-sphere model using a sphere diameter of L, and a sphere volume fraction equal to the volume fraction of the fd-virus.

shown that the method can be considered as a means to probe the equation of state and the structural correlations of the background complex fluids.

3. Entropically driven particle motion and self-assembly

The experiments described in § 2 quantitatively establish that entropic forces are significant, and are strongly influenced by correlation effects in the background complex fluid. It is not surprising that the entropic forces are significant. Depletion-driven aggregation and phase separation have been observed in many systems. In this section we discuss some of our recent research along these lines, culminating in experiments that combine surface structure and entropy to produce highly ordered colloidal crystals.

In pure particle suspensions, for example mixtures of large and very small colloidal spheres, most experimental and theoretical evidence indicates that first-order fluid–solid phase transitions occur in the bulk (Dinsmore *et al.* 1995; Kaplan *et al.* 1994; Dinsmore *et al.* 1997; Imhof & Dhont 1995; van Duijneveldt *et al.* 1993; Rosenfeld 1994; Poon & Warren 1994; Sanyal *et al.* 1992; Biben & Hansen 1991). Experiments have determined transition volume fractions in samples with differing particle type, size and size ratio. In figure 8*a* we show a phase diagram and some data (Dinsmore *et al.* 1995) from samples composed of *ca.* 800 nm diameter polystyrene spheres and *ca.* 70 nm diameter polystyrene spheres. At small total volume fraction the suspension

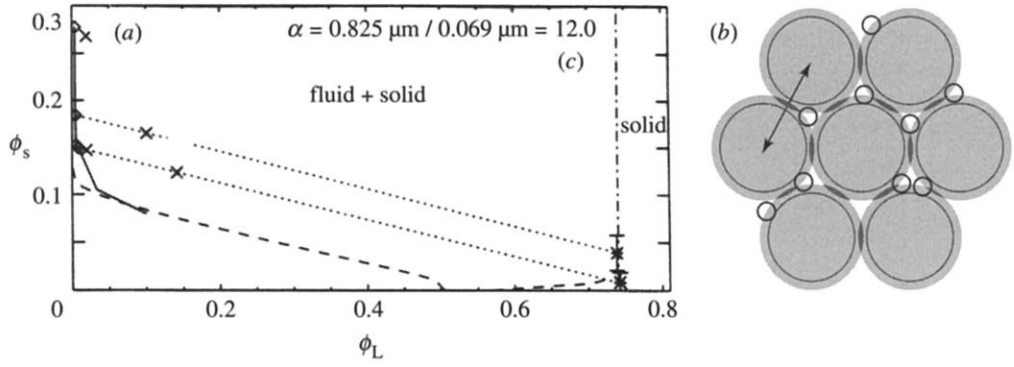

Figure 8. (*a*) Experimental phase diagram (solid line and points) and theory (dashed and dot-dashed line) for the binary hard-sphere colloid described in the text. (*b*) Cartoon of the solid phase modelled by the theory.

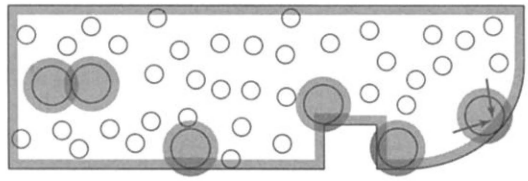

Figure 9. Schematic of the depletion effect in various geometries. The dark shaded region represents the gain of small-sphere excluded volume (entropy).

is a fluid mixture of different-sized hard spheres, but when the small-sphere volume fraction is increased sufficiently, the mixture phase separates into a large-ball-poor hard-sphere fluid and a large-ball-rich colloidal crystal. The dotted lines are tie lines. The dashed lines are predictions of a simple theory (Dinsmore *et al.* 1995) that treated the fluid phase as a mixture of large and small hard spheres, deriving the pressure of the fluid from the Carnahan–Starling equation of state (Carnahan & Starling 1969), and treated the solid phase as an FCC crystal of large spheres permeated by a fluid of small hard-spheres (see figure 8*b*). The driving force for crystallization is made apparent in figure 8*b*; when the lattice constant of the FCC crystal decreases, the regions of excluded volume overlap more, and thus create more entropy for the fluid of small spheres.

While carrying out these systematic experiments on binary colloidal suspensions, we discovered (Kaplan *et al.* 1994) that the first instability arising in many binary particle mixtures was phase separation into an ordered *surface* phase and a disordered *bulk* liquid phase. Disordered and ordered surface phases can also be understood using simple excluded-volume entropy arguments, in this case between the large particle and the wall (depicted in figure 9). The entropic force on a particle near the wall surface is roughly twice as large as that between two large particles in the bulk!

In figure 10*a–d* we use a series of pictures to convey the general systematics of these effects. The samples were composed of large (*ca.* 0.8 μm diameter) and small (*ca.* 0.07 μm diameter) polystyrene spheres suspended in water. The system was salted at a concentration of *ca.* 0.01 M so that particle interactions were approximately hard sphere. The water was a mixture of D_2O and H_2O in order to create

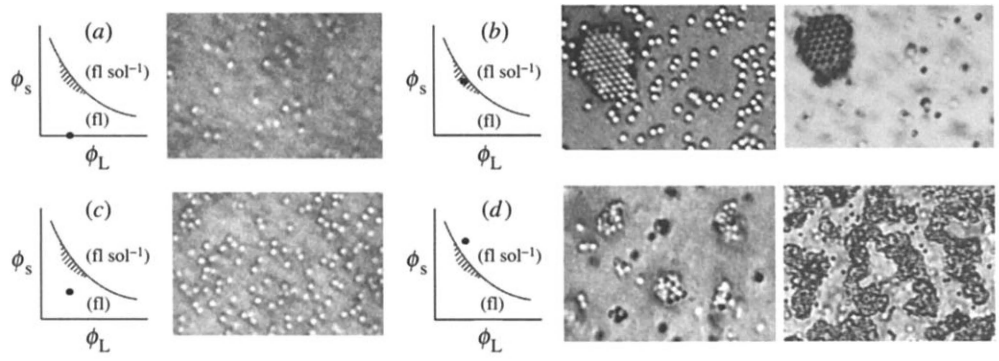

Figure 10. Microscope images of 0.825 μm/0.069 μm diameter binary particle suspensions as a function of small-ball volume fraction Φ_S. The large ball volume fraction is held constant at $\Phi_L = 0.02$, and only the large balls are apparent in the images. To the left of each photo we show the sample preparation volume fractions (the dots) along with the liquidus line. Parts (*a*)–(*c*) are imaged on the surface just below the cell wall, and part (*d*) is imaged *ca.* 20 μm into the bulk sample. (See text for further discussion.)

near-neutral buoyancy conditions for polystyrene. The large-ball volume fraction was fixed at $\Phi_L = 0.02$, and the small-sphere volume fraction was varied. We designed a small glass sample cell (*ca.* 100 μm thick) so that the large particles in these suspensions could be observed in real time using our optical microscope. To the left of each photograph is a 'quasi-phase diagram', indicating the volume fraction of large and small spheres, as well as our estimated liquidus line. In figure 10*a–c* the focal plane was chosen just beneath the sample cell wall in order to reveal surface growth dynamics, and in figure 10*d* we chose a slice within the cell in order to reveal the bulk growth dynamics.

We see that the large-particle concentration increases on the wall surface with increasing small-sphere volume fraction, and that surface crystallization begins in a region of the phase diagram just below the liquidus line (note, the lifetime of the large particles on the wall also increases dramatically (much greater than 10^3) between 10*a* and 10*b*). The crystalline structure grows rapidly along the wall, and more slowly into the bulk. In figure 10*c* we show an image (rightmost) of the second layer of the surface crystal; notice the number density of large particles in the background fluid is much less than on the surface. For samples prepared with volume fractions above the liquidus line (figure 10*d*), a rapid nucleation of large ball clusters is revealed (in less than 10 min). These clusters typically sediment or combine to form a gel (rightmost image of figure 10*d*). Thus there exist interesting windows of opportunity in these low-volume-fraction entropically driven systems, wherein high-quality particle assembly is possible, free of bulk complications.

We have learned that entropic excluded volume effects induce attractions between particles and even stronger attractions between particles and walls. Can similar effects be used to position particles on substrates or move them in a predetermined way? The answer is yes. Geometric features on a surface can create *entropic force fields* that trap, repel or induce drift of the larger particles in suspension (Dinsmore *et al.* 1996). Large particles, moving in the vicinity of steps, grooves, or corners cut into a flat substrate, modify the small-sphere free volume in a manner dependent on large-particle position and on the size and shape of the geometric features (see

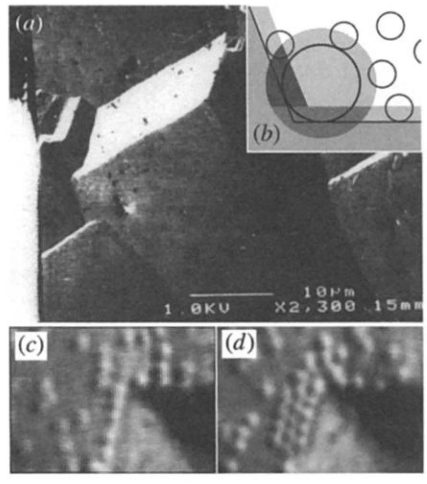

Figure 11. (*a*) Scanning electron microscope image of the surface of our silicon wafer showing facets. (*b*) Schematic of the depletion effect in a corner. (*c*) Particles assembling along the facet corner. (*d*) The same sample 10 min later. A two-dimensional crystallite has formed and is aligned with the corner. The sample consisted of *ca.* 500 nm and *ca.* 83 nm polystyrene spheres in water. $\Phi_S = 0.35$ and $\Phi_L = 0.30$.

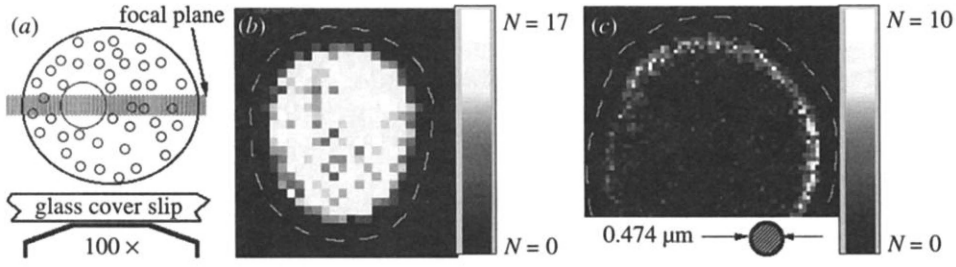

Figure 12. (*a*) Cartoon of a 600 nm thick slice through a 1-stearoyl-2-oleoyl-sn-glycero-3-phosphocholine vesicle imaged with an optical microscope. We measured the in-plane positions of the larger colloidal sphere when it was in focus. (*b*) Shaded regions represent the probability distribution of a single 0.237 μm radius polystyrene sphere inside a vesicle (no small spheres). Lighter shading denotes higher probability. The white dashed line is the edge of the vesicle, and the shading indicates the number of times, N, the centre of the sphere was observed in a bin located at a given point. There were 2000 events and the bins were 130×130 nm^2. The sphere simply diffused freely throughout all of the available space. (*c*) Same as (*b*), but with a vesicle that also contained small spheres ($\Phi_S = 0.30$, $\frac{1}{2}a_S = 0.042$ μm). There were 2300 events and the bin size was 65 nm. The large sphere was clearly attracted to the vesicle wall, especially where the vesicle was most curved.

figure 9 for schematic examples). We have observed and quantified these phenomena at step edges (Dinsmore *et al.* 1996), near corners (Dinsmore & Yodh 1999), and in vesicles (Dinsmore *et al.* 1998).

Some examples of these surface structure effects are illustrated in figures 11 and 12. In figure 11 we exhibit the depletion-driven behaviour of large polystyrene particles near a corner. The corners are formed from naturally occurring facets on the backside of a silicon wafer. A corner is composed of two walls, and its entropic attraction

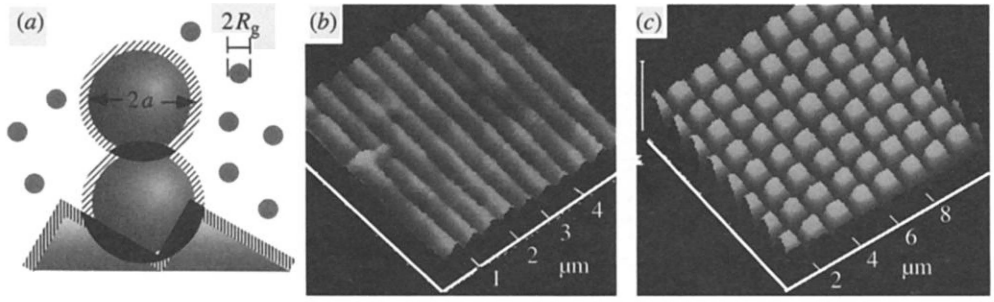

Figure 13. (*a*) The depletion effect. The centres of non-adsorbing polymer coils (small spheres) are excluded from a depletion zone (hashed regions) outside the large spheres and corrugated walls. Spheres are preferentially drawn to interior corners. Atomic force microscope images of (*b*) the replica optical grating (i.e. the one-dimensional template) in PMMA, and (*c*) the crossed grating (i.e. the two-dimensional template).

is twice as large as on the flat part of the wall. The micrographs demonstrate 'pre-freezing' of large spheres in the corner. Notice that the corner also aligns colloidal crystals along a specific direction in the plane, a potentially useful feature when making ordered arrays of particles on a chip. In figure 12 we explore the behaviour of binary hard-sphere suspensions within vesicles. We quantified this behaviour by measuring the number of times a large sphere appeared at different in-plane positions within the vesicle. With added small spheres we find the large particles are pushed to the vesicle walls, and even to regions with higher curvature along the walls. Thus, the depletion scheme provides a mechanism to drive large macromolecules to membrane surfaces, to keep them at the surface for longer times, and even to 'push' them to specific locations along the surface. These basic ideas are not limited to binary hard-sphere colloids, but are extendable to 'lock-and-key' steric interactions on macromolecular length-scales and to the behaviour of complex fluids in porous media.

Building on these demonstrated effects, it is possible to devise arrays of such structures that can be used to self-assemble particles in a chosen pattern. Our concluding example demonstrates this idea, thus introducing a qualitatively new approach to colloidal epitaxy based on equilibrium thermodynamics and geometry (Lin *et al.* 2000). We used templated surfaces with spatially periodic one-dimensional and two-dimensional height profiles to create a periodic surface potential, and then to drive the growth of two- and three-dimensional particle structures nucleating from these templates. The template was created by making an imprint of a diffraction grating in a thin polymer film (see figure 13). Spheres in contact with two (four) flat walls of the grating groove experience an attractive force up to four (eight) times the two-sphere value in the bulk, depending on the exact geometry. The large spheres are thus forced to the grating valleys. Imprint or stamping techniques provide a simple way of making replicas of surface structures (Chou *et al.* 1996; Xia *et al.* 1996). In figure 13 we show an atomic force microscope (AFM) image of a replica optical grating in a *ca.* 400 nm thick PMMA film. By rotating the substrate 90° and imprinting a second time, we create two-dimensional periodic structures, resembling an array of square pyramids. The templates form one wall of the sealed sample chambers, which are 30–100 μm thick and contain a few microlitres of sample.

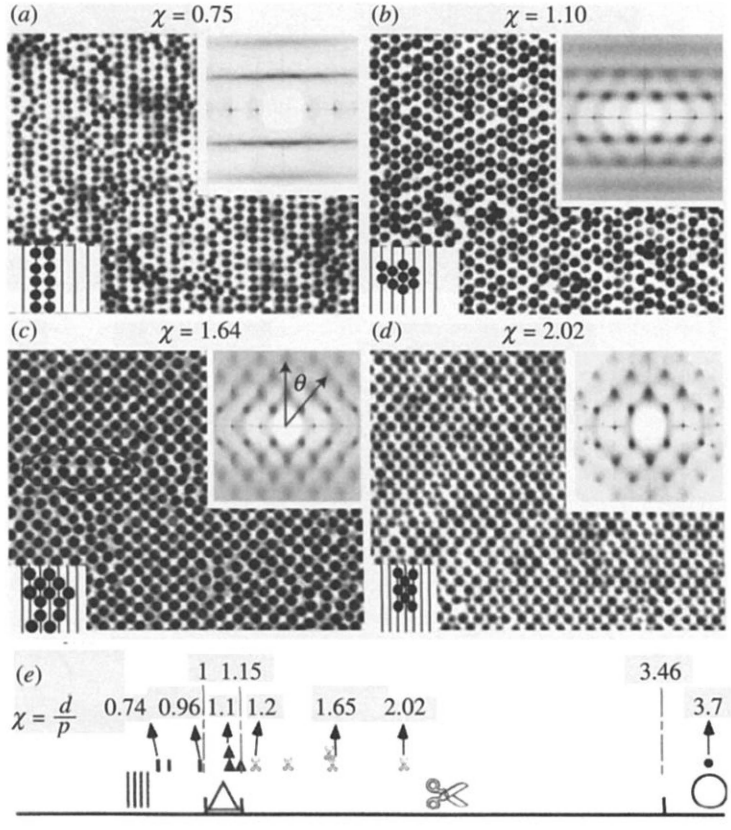

Figure 14. Phase-contrast micrographs of four representative two-dimensional structures with the schematic reconstruction in the bottom left corner. The structure function $S(k)$ computed from these images is shown in the top right corner. (*a*) Stripe phase, (*b*) triangular phase, (*c*), (*d*) scissor (centred-rectangular) phases with different scissor angles as defined in the structure function image of (*c*). In (*c*) we circle the mirror line of a twinning defect. (*e*) Diagram indicating the observed phases as a function of $\chi = d/p$.

The samples consisted of 0.7–1.2 μm diameter PMMA spheres stabilized by a grafted layer of poly-12-hydroxy stearic acid (Antl *et al.* 1986; Ilett *et al.* 1995). In an organic solvent mixture of decalin/cyclohexylbromide, these spheres are nearly density matched with a refractive index mismatch of less than 0.01. Such small index mismatches reduce light scattering, facilitating optical microscopy deep into the suspension. Depletion attractions were induced by adding polystyrene polymer, with a radius of gyration, $R_g \sim 15$ nm ($M_w = 320\,000$, $M_w/M_n = 1.04$, Polymer Laboratories). We scaled the concentration of polymer used with different-sized spheres to keep the free energy reduction at contact fairly constant.

This novel colloidal system offers a fascinating new testing ground for the investigation of two-dimensional assembly and phase transitions. In figure 14 we exhibit phase contrast micrographs of four representative two-dimensional structures that entropically assembled on the one-dimensional entropic grating potentials. The concentrations of spheres and polymer were adjusted in this case so that bulk crystallization did not occur. The results vary as a function of the ratio of the mean interparti-

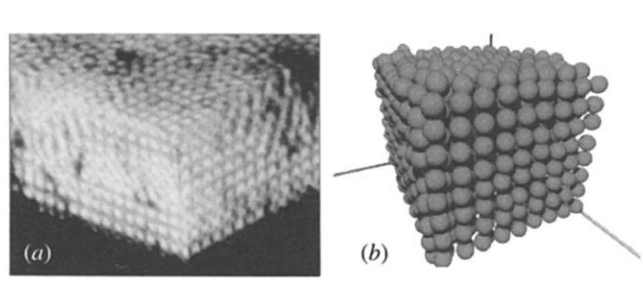

Figure 15. (*a*) Three-dimensional confocal image showing 20 layers within the interior of a greater than 30 layer FCC colloidal crystal grown on a $d/p = 1$ crossed-grating entropic template. (*b*) Computer reconstruction of the lattice based on particle coordinates determined from the microscope images.

cle spacing, d (which was usually somewhat larger than the particle diameter), to the grating period, p. Briefly, when $d < p$, one-dimensional colloidal liquids form in the grooves of the template. As the particle size is increased, the one-dimensional colloidal liquids of adjacent rows interact more strongly, and hexagonal symmetry emerges in two dimensions. Ordered structures are maintained with hexagonal order giving way to centred rectangular symmetry as d/p is further increased. Finally, at the largest d/p ratios, the particles are too big to experience the entropic effects of surface roughness, and the surface structure becomes disordered. All of the ordered structures exhibited diffuse scattering peaks (see insets of micrographs) characteristic of bond-angle ordered phases in an aligning field, rather than power-law peaks characteristic of two-dimensional crystal order.

Finally, the two-dimensional (crossed) entropic grating potentials offer us the possibility of assembling high-quality three-dimensional face-centred cubic (FCC) crystals. To achieve this goal, the ratio d/p is adjusted to unity. This template potential nucleates the [100] face of an FCC crystal. Growth from this face insures that the stacking of layers is not random (e.g. as is the case for nucleation from a flat surface) (van Blaaderen *et al.* 1997). In figure 15 we show a confocal microscopy image of 20 layers within the interior of a *ca.* 30–40 layer FCC crystal. Also shown is a reconstruction of the lattice based on the coordinates of the particles determined from the microscope images.

The combination of depletion attraction and simple geometric templating thus provides a qualitatively new route for controlled self-assembly of high-quality colloidal crystals. Since the scheme employs an equilibrium process, it will work with any kind of 'nearly hard-sphere' particle under appropriate suspension conditions. Furthermore, since the entropic principles used here are not restricted to micron-sized particles, the underlying principles should be applicable on smaller macromolecular length-scales to other soft materials and even to biological systems, such as the crowded interior environment of a cell.

We have had the good fortune to work with many outstanding scientists on this research over the past few years. We particularly thank Dave Pine, Tom Lubensky, Dave Weitz, Phil Nelson, Jennifer Rouke, Joe Matteo, Derek Wong, Vikram Prasad, Andrew Schofield, Patrick Warren and Wilson Poon for their collaboration. We also thank Zigurts Majumbdar, Andrew Levitt, Josh Gruber, Jian Zhang, Rachel Owen, Subrata Sanyal, Evan Hohlfeld, Eric Weeks, Dennis Discher, Dan Hammer, Ahmed Sinai and Mohammad Islam for valuable discussions and technical assistance that affected many aspects of this research. This work was supported by NASA

grant NAG3-2172, and by the National Science Foundation through grant DMR99-71226 and the PENN NSF-MRSEC grant DMR-96-32598.

References

Adams, M., Dogic, Z., Keller, S. L. & Fraden, S. 1998 *Nature* **393**, 349.

Afzal, R. S. & Treacy, E. B. 1992 *Rev. Sci. Instrum.* **63**, 2157.

Antl, L., Goodwin, J. W., Hill, R. D., Ottewill, R. H., Owens, S. M., Papworth, S. & Waters, J. A. 1986 *Colloids Surf.* A **17**, 67–78.

Arutyunyan, A. V., Ivanova, M. A., Kurlyand, D. I. & Noskin, V. A. 1993 *Molec. Biol.* **27**, 705–712.

Asakura, S. & Oosawa, F. 1958 *J. Polym. Sci.* A **33**, 1983.

Ashkin, A., Dziedzic, J. M., Bjorkholm, J. E. & Chu, S. 1986 *Opt. Lett.* **11**, 288.

Baumann, C. G., Smith, S. B., Bloomfield, V. A. & Bustamante, C. 1997 *Proc. Natl Acad. Sci. USA* **96**, 6185–6190.

Biben, T. & Hansen, J. P. 1991 *Phys. Rev. Lett.* **66**, 2215–2218.

Biben, T., Bladon, P. & Frenkel, J. 1996 *Physica* B **8**, 10 799.

Bibette, J., Roux, D. & Nallet, F. 1990 *Phys. Rev. Lett.* **65**, 2470–2473.

Bibette, J., Roux, D. & Pouligny, B. 1992 *J. Phys.* B **2**, 401–424.

Bolhuis, P. G., Stoobants, A., Frenkel, D. & Lekkerkerker, H. N. W. 1997 *J. Chem. Phys.* **107**, 1551.

Calderon, F. L., Bibette, J. & Biais, J. 1993 *Europhys. Lett.* **23**, 653–659.

Carnahan, N. F. & Starling, K. E. 1969 *J. Chem. Phys.* **51**, 635.

Chou, S. Y., Krauss, P. R., Zhang, W., Guo, L. J. & Zhuang, L. 1996 *J. Vac. Sci. Technol.* B **15**, 2897–2904.

Chu, X. L., Nikolov, A. D. & Wasan, D. T. 1996 *Langmuir* **12**, 5004.

Crocker, J. C., Matteo, J. A., Dinsmore, A. D. & Yodh, A. G. 1999 *Phys. Rev. Lett.* **82**, 4352.

Dauson, J. R. & Harpst, J. A. 1971 *Biopolymers* **10**, 2499.

De Hek, H. & Vrij, A. 1981 *J. Colloid Interface Sci.* **84**, 409.

Dickman, R., Attard, P. & Simonian, V. 1997 *J. Chem. Phys.* **107**, 205.

Dinsmore, A. D. & Yodh, A. G. 1999 *Langmuir* **15**, 314–316.

Dinsmore, A. D., Yodh, A. G. & Pine, D. J. 1995 *Phys. Rev.* E **52**, 4045.

Dinsmore, A. D., Yodh, A. G. & Pine, D. J. 1996 *Nature* **383**, 239–242.

Dinsmore, A. D., Warren, P. B., Poon, W. C. K. & Yodh, A. G. 1997 *Europhys. Lett.* **40**, 337–342.

Dinsmore, A. D., Wong, D. T., Nelson, P. & Yodh, A. G. 1998 *Phys. Rev. Lett.* **80**, 409–412.

Dogic, Z. & Fraden, S. 1997 *Phys. Rev. Lett.* **78**, 2417–2420.

Faucheux, L. P., Bourdieu, L. S., Kaplan, P. D. & Libchaber, A. 1995*a* *Phys. Rev. Lett.* **74**, 1504.

Faucheux, L. P., Stolovitzky, G. & Libchaber, A. J. 1995*b* *Phys. Rev.* E **51**, 5239.

Fraden, S., Maret, G. & Caspar, D. L. D. 1993 *Phys. Rev.* E **48**, 2826–2837.

Gast, A. P., Hall, C. K. & Russel, W. B. 1983 *J. Colloid Interface Sci.* **96**, 251.

Gotzelmann, B., Evans, R. & Deitrich, S. 1998 *Phys. Rev.* E **57**, 6785.

Grosberg, A. Y. & Khokhlov, A. R. 1994 In *Statistical physics of macromolecules.* New York: AIP.

Ilett, S. M., Orrock, A., Poon, W. C. K. & Pusey, P. N. 1995 *Phys. Rev.* E **51**, 1344–1352.

Imhof, A. & Dhont, J. K. G. 1995 *Phys. Rev. Lett.* **75**, 1662.

Joanny, J. F., Leibler, L. & DeGennes, P. G. 1979 *J. Polym. Sci.* A **17**, 1073.

Kaplan, P. D., Rouke, J. L., Yodh, A. G. & Pine, D. J. 1994 *Phys. Rev. Lett.* **72**, 582.

Lin, K.-H., Crocker, J. C., Prasad, V., Schofeld, A., Weitz, D. A., Lubensky, T. C. & Yodh, A. G. 2000 *Phys. Rev. Lett.* **85**, 1770–1773.

Mao, Y., Cates, M. E. & Lekkerkerker, H. N. W. 1995 *Physica* A **222**, 10–24.

Mao, Y., Bladon, P., Lekkerkerker, H. N. W. & Cates, M. E. 1997 *Molec. Phys.* **92**, 151.

Pernodet, N. & Tinland, B. 1997 *Biopolymers* **42**, 471–478.

Piasecki, J., Bocquet, L. & Hansen, J.-P. 1995 *Physica* A **218**, 125.

Poon, W. C. K. & Warren, P. B. 1994 *Europhys. Lett.* **28**, 513.

Poon, W. C. K., Ilett, S. M. & Pusey, P. N. 1994 *Nuovo Cim.* D **16**, 1127–1139.

Poon, W. C. K., Pirie, A. D., Haw, M. D. & Pusey, P. N. 1997 *Physica* A **235**, 110–119.

Rosenfeld, Y. 1994 *Phys. Rev. Lett.* **72**, 3831.

Sanyal, S., Easwar, N., Ramaswamy, S. & Sood, A. K. 1992 *Europhys. Lett.* **18**, 107–110.

Schaefer, D. W., Joanny, J. F. & Pincus, P. 1980 *Macromolecules* **13**, 1280–1289.

Schmidt, R. L. 1973 *Biopolymers* **12**, 1427–1430.

Smith, W. 1970 *J. Chem. Phys.* **52**, 953–960.

Steiner, U., Meller, A. & Stavans, J. 1995 *Phys. Rev. Lett.* **74**, 4750–4753.

Stroobants, A., Lekkerkerker, H. N. W. & Odijk, T. 1986 *Macromolecules* **19**, 2232–2238.

Tang, J. X. & Fraden, S. 1995 *Liq. Cryst.* **19**, 459–467.

Taylor, W. H. & Hagerman, P. J. 1990 *J. Molec. Biol.* **212**, 363–376.

van Blaaderen, A., Ruel, R. & Wiltzius, P. 1997 *Nature* **385**, 321.

van Bruggen, M. P. B., van der Kooij, F. M. & Lekkerkerker, H. N. W. 1996 *J. Phys. Condens. Matter* **8**, 9451–9456.

van Duijneveldt, J. S., Heinen, A. W. & Lekkerkerker, H. N. W. 1993 *Europhys. Lett.* **21**, 369–374.

Verma, R., Crocker, J. C., Lubensky, T. C. & Yodh, A. G. 1998 *Phys. Rev. Lett.* **81**, 4004.

Verma, R., Crocker, J. C., Lubensky, T. C. & Yodh, A. G. 2000 *Macromolecules* **33**, 177–186.

Vliegenthart, G. A. & Lekkerkerker, H. N. W. 1999 *J. Chem. Phys.* **111**, 4153.

Vrij, A. 1976 *Pure Appl. Chem.* **48**, 471.

Xia, K. E., Zhao, X. M., Rogers, J. A., Prentiss, M. & Whitesides, G. M. 1996 *Science* **273**, 347–349.

Yaman, K., Jeppesen, C. & Marques, C. M. 1998 *Europhys. Lett.* **42**, 221–226.

Discussion

J.-P. HANSEN (*Department of Chemistry, University of Cambridge, UK*). Do you believe that it would be possible to induce an amorphous glass phase in a colloidal dispersion by the use of a disordered substrate or template?

A. G. YODH. Your suggestion is a very interesting one. I think it may be impossible to induce a metastable amorphous phase. I think it is an experiment worth trying, because it will be interesting either way.